

Bayesian estimation of englacial radar chronology in Central West Antarctica

Gail R. Muldoon,¹ Charles S. Jackson,¹ Duncan A. Young,¹ and Donald D.

Blankenship¹

¹Institute for Geophysics, University of

Texas at Austin, Austin, Texas, USA.

Abstract. Englacial radar reflectors in the central West Antarctic Ice Sheet (WAIS) contain information about past dynamics and ice properties. Thanks to significant data coverage in this area, these isochronous reflectors can be traced over large portions of the ice sheet, but assigning ages to the reflectors for the purpose of studying dynamics requires incorporation of chronologic data from ice cores. To date reflectors in the Marie Byrd Land region, we consider the Byrd ice core, strategically located between the catchments of Thwaites Glacier and the Siple Coast ice streams. However, the deep Byrd ice core chronology lacks uncertainty estimates which are important to confidently date far-reaching englacial isochrones.

Here we determine ages with uncertainty for a series of four englacial radar reflectors spanning the ice thickness using Bayesian approaches to combine data and uncertainty information from radar observations, an existing Byrd ice core chronology, and a simplified ice sheet model. This method returns a posterior representing the probability distribution of depth and age for observed radar reflectors while allowing for correlation of errors between ice sheet parameters with depth. We present a complete age-depth profile estimate with uncertainty for the Byrd ice core which compares favorably with the more recent WAIS Divide ice core record. Our results estimate ice sheet parameters such as accumulation rate history and suggest the deepest continuous radar reflector is approximately 25.42 ± 2.49 ka, far younger than the estimated age recorded at the bottom of the ice core.

1. Introduction

Isochronous, englacial radar reflectors can map the age structure of an ice sheet, with the thickness of layers bounded by reflectors revealing information about ice flow dynamics and changing ice properties. To date englacial radar reflectors, it is necessary to tie them to a known chronology, such as at an ice core site as has been done elsewhere [Cavitt et al., 2016]. Dated englacial radar observations enables information from the entire ice volume—in addition to surface observations—to constrain ice dynamics in the central WAIS, including the fast-changing Thwaites Glacier catchment. More than three extensive radar surveys passing near the Byrd ice core site, including the recent GIMBLE project, make the Byrd ice core particularly useful for dating paleo ice dynamics observed in the central WAIS.

To understand how well radar reflectors can be dated, we use Bayesian methods to synthesize information from ice cores, radar sampling, ice flow modeling, and our knowledge of the leading sources of uncertainty. We apply our approach to the central West Antarctic ice sheet, an area of concentrated radar surveys and the location of the Byrd ice core [Gow et al., 1968]. The proximity of the Byrd ice core (80.0167°S , 119.5167°W) to fast-changing ice of both the Siple and Amundsen Sea coasts in West Antarctica makes it a potentially important source of information in studies of the response of the West Antarctic Ice Sheet (WAIS) to changing climatic conditions.

While the Byrd ice core has been dated to more than 90ka [Blunier and Brook, 2001], nearly back to the Last Interglacial, there are currently no robust estimates of uncertainty in the Byrd ice core chronology. Quantifying such uncertainty is challenging because

it arises from a number of sources, including measured depth and age of the ice and unknown ice flow parameters. This problem is nontrivial because age-depth solutions are nonunique and depend on solutions elsewhere in the ice column. Despite this, it is important to include uncertainty in the Byrd ice core chronology when using it to characterize the englacial age structure of the greater West Antarctic Ice Sheet (WAIS) to limit the propagation of unrealistic certainty in age, particularly at depth where shear thinning is dominant and uncertainties are expected to be greatest.

We use a novel approach to probabilistically date englacial radar reflectors observed near the Byrd ice core given information about the radar-observed two-way travel time (TWTT), previously-computed age-depth observations of the ice core, constraints on englacial stratigraphy, and other factors. A simple flow model is used to show how age of the reflectors varies with depth, taking into account our knowledge of ice flow physics and surface accumulation rate. While some information about these parameters is known, large uncertainties remain. To account for these and nonunique solutions of the age-depth chronology, we use a probabilistic method to estimate uncertainty in the parameter values to find combinations of parameter values which lead to age-depth solutions consistent with observations.

Section 2 discusses the formulation of the Bayesian problem and methods for finding solutions of the age and depth of observed englacial radar reflectors. Section 3 shows results for the probability distributions of reflector age and depth as well as a comparison to the WAIS Divide ice core chronology as an independent check on our results.

2. Posterior distribution of englacial reflector age-depth

In order to assign ages to observed radar reflectors, we are interested in combining information from radar, ice flow physics, and ice cores to derive an age-depth profile of ice at the Byrd ice core site. To derive this updated chronology with uncertainty, we compute the age of englacial reflectors given information about radar-observed TWTT, local ice flow, and a volcanic chronology of the ice core.

We represent the solution as an ensemble because the presence of non-unique solutions necessitates a probabilistic approach. To estimate the age-depth profile at the Byrd ice core, we use Bayesian calibration to invert for the age and depth of observed englacial radar reflectors. This problem is nontrivial because the age of each reflector depends on solutions elsewhere in the ice column, so they are correlated to each other with depth.

This method preserves the chronologic superposition of the ice column and correlation of errors with depth, estimates the probability of ice flow parameter values, and develops a probabilistic estimate of the age-depth profile. A probabilistic approach is useful because while some parameters are well known, others are highly uncertain, such as the accumulation function at this site over time. By iteratively inverting for non-unique solutions, we find a distribution of sets of parameter values which are consistent with observations. Specifically, we derive an ensemble of age-depth profiles for the Byrd ice core constrained by agreement with a chronology of volcanic events from the past 50,000 years detected in the Byrd ice core record using the electrical conductivity method [Hammer *et al.*, 1997] and with TWTT to bright, continuous reflectors observed in ice-penetrating radar [Holt *et al.*, 2006; Young *et al.*, 2012; Morse *et al.*, 2002] and traced using Landmark seismic interpretation software produced by Halliburton.

The Bayesian formulation of this problem is:

$$\begin{aligned} p(A_r) \sim p(D_r, \vec{f}, d_{firn}, v_{ice}, S | TWTT_r, A_{IC}, D_{IC}) \propto \\ p(D_r, f, S) \cdot p(d_{firn}) \cdot p(v_{ice}) \cdot p(A_{IC}, D_{IC} | \vec{f}, S) \cdot p(TWTT_r | D_r, d_{firn}, v_{ice}) \end{aligned} \quad (1)$$

Computing the posterior probability distribution of reflector ages (far left in Equation 1 requires estimating the depths of the englacial reflectors of interest (D_r), ice flow model parameters (\vec{f}), firn depth correction (d_{firn}), radar velocity in ice (v_{ice}), and precision of the Byrd ice core chronology (S). We estimate these values given information about observed radar reflector two-way travel time ($TWTT_r$) and the age-depth profile from the Byrd ice core volcanic record (A_{IC} , D_{IC}).

Priors, the first three terms on the right-hand side of Equation 1, are used to put physical bounds on estimates of quantities of interest as described in the following sections. Priors on D_r also preserve stratigraphic dependence of radar reflectors, requiring deeper reflectors be older than shallower reflectors. Likelihood functions, the remaining two factors on the right-hand side of Equation 1, describe the probability that modeled results agree with observations. In the first, agreement between flow model results (\vec{f}) and the volcanic record (A_{IC}, D_{IC}) given precision (S) and in the second, agreement between observed two-way travel time ($TWTT_r$) and modeled reflector depths (D_r) given information about the local firn correction (d_{firn}) and radar velocity in ice (v_{ice}). These elements of Equation 1 are discussed more thoroughly in subsequent sections.

Accepted solutions are expected to satisfy all of these conditions simultaneously, so we take the product of their probabilities in Equation 1. The Metropolis algorithm is used to identify combinations of parameters and boundary conditions consistent with observations and sources of uncertainty. To do so, sets of parameter values for D_r , \vec{f} , S , d_{firn} , and v_{ice} are proposed using a markov chain method as in Equation A1. Likelihood functions for age

and TWTT are evaluated to accept or reject these proposed parameter sets based on how well they agree with data. Solutions are those parameter sets which are simultaneously consistent with physical limits defined by the priors and with uncertain observations.

The resulting posterior probability distribution, $p(D_r, \vec{f}, S | TWTT_r, A_{IC}, D_{IC})$, can then be used to deterministically compute the corresponding probability distribution of the age of observed radar reflectors, $p(A_r)$, using the flow model described below.

2.1. Ice flow model at the Byrd ice core

Due to the inherent stratigraphic dependence of age in the ice column and the nonlinear effect of ice deformation on layer depths, we use a flow model to simulate the age-depth relationship. We use a simple, one-dimensional model of ice flow (Equation 2) which derives ice age from accumulation and strain rate, assuming constant horizontal strain rate in the upper part of the ice sheet and a shear layer of thickness h at the bottom of the ice sheet [Schwander *et al.*, 2001]. In the shear layer, the strain rate is assumed to decrease linearly and the bottom of the ice is assumed sliding with velocity $q \cdot v_0$, where v_0 is the horizontal velocity at the surface.

$$A(z) = \int_z^H \frac{dz}{\epsilon_z \cdot \dot{a}(z)} \quad (2)$$

where

$$\epsilon_z = \begin{cases} 1 - k(H - z), & h \leq z \leq H \\ kz(q + \frac{1-q}{2h}z), & 0 < z < h \end{cases},$$

$$k = \frac{2}{2H - h(1-q)}$$

H is ice thickness in ice equivalent, which has been observed to be 2164 m at the Byrd ice core site; z is the height above the bed, i.e. the inverse of H . We invert for the remaining parameters: h , the depth to the Dansgaard-Johnsen shear layer, \dot{a} the accumulation rate

which is expressed as a piecewise function with 11 depth bins (see below), and q , the ratio of horizontal velocity at the surface and bed of the ice sheet.

The ice flow model accounts for two primary factors in the age-depth profile: burial as a function of accumulation rate, \dot{a} , and thinning as a function of strain, ϵ_z . In the simplest realization, ice deposited at a given time at the ice sheet surface will be found at a depth in the ice sheet corresponding to the amount of subsequent accumulation. However, due to strain thinning at depth, the ice will be less deep than would be expected if accumulation alone is considered.

As described in Section 2.3, we invert for the flow parameters h , q , and \dot{a} . Constant values for h and q are sampled from uniform priors defined in a conservative range. Accumulation rate, \dot{a} , is estimated for 11 units of depth spaced every 200 m starting from the ice surface and are sampled from the same uniform prior.

$$p(\vec{f}) = \begin{cases} p(h) \sim U(0, 0.5) \\ p(q) \sim U(0, 1) \\ p(\dot{a}_{d=11}) \sim U(0.5m/a, 0.25m/a) \end{cases} \quad (3)$$

The prior distributions of flow parameters, together denoted as $p(\vec{f})$, conservatively assume the shear layer is in the bottom half of the ice sheet depth [Cuffey and Paterson, 2010] and that the bed of the ice sheet is moving no faster than the surface, which would allow for cases of both plug and creep flow. Accumulation rate as a function of depth, \dot{a} , is sampled from 11 distinct depth bins spanning the ice thickness with transition depths at 200, 400, 600, 800, 1000, 1200, 1400, 1600, 1800, and 2000 m. This allows for variability of accumulation over time. To limit unrealistic variability in accumulation between depth bins, Tikhonov regularization is used on the age likelihood function to punish estimates

of the accumulation function which are highly variable. This term appears in Equation 5 as is described further in Appendix B.

2.2. Radar depth and error

In addition to constraining the age of englacial reflectors with the Byrd ice core chronology, we also quantify uncertainty in their radar-observed depth, another source of error in the age-depth profile. The ice-penetrating radar used in this analysis was collected in several surveys conducted by the University of Texas Institute for Geophysics, including GIMBLE [Young *et al.*, 2012], CASERTZ [Morse *et al.*, 2002], and SOAR/WMB [Luyendyk *et al.*, 2003]. Data has been collected from a DC-3 or Twin Otter airborne platform and uses the HiCARS radar system with 60 MHz center frequency and 15 MHz bandwidth [Peters *et al.*, 2005]. Radar pulses transmitted into the ice sheet reflect off surfaces of dielectric contrast in the ice which are the result of variations in ice fabric, composition, temperature, rheology, etc [Fujita *et al.*, 2000]. The reflected signal is received by the radar system and recorded as two-way travel time (TWTT) from transmission to receipt.

In this study, we consider TWTT of four reflectors spanning the ice thickness in the region of central West Antarctica (Figure 2). These reflectors have been tracked extensively using Halliburton's Landmark seismic interpretation software and can be tied to both the Byrd and WAIS Divide ice cores for dating.

To estimate reflector depths, D_r , we begin with a simple relation assuming known velocity of the signal in air and in ice (first term in Equation 4). We also incorporate several known sources of uncertainty, including: 1) variations in the signal velocity in ice due to ice temperature and fabric, 2) vertical resolution limitations resulting from

digitized pulse width sampling effects, and 3) measurement errors in the density profile needed to account for the changing signal velocity in firn (Equation 4).

$$D_i = \frac{1}{2} TWTT \cdot \vec{v} + \epsilon_{v_{ice}} + \epsilon_{PW} + \epsilon_{firn} \quad (4)$$

The first source of error, $\epsilon_{v_{ice}}$, results from ice temperature, crystal structure, anisotropy, and other ice fabric effects. EM velocity in ice, v_{ice} , varies from 168 to 169.5 m/ μ s [Fujita et al., 2000] and the integration of these errors leads to increasing uncertainty with depth. The complexity of local ice properties affecting the velocity at any location and depth make it difficult to know the error distribution, so we make the simplifying and conservative assumption that this error is uniform. Constant values of v_{ice} are therefore sampled from a uniform distribution: $p(v_{ice}) \sim U(168m/\mu s, 169.5m/\mu s)$.

The radar pulse width determines its vertical resolution [Millar, 1982]. We assume a finite pulse width, meaning that an infinitesimally thin layer of ice will appear in the survey to have a finite width. This can lead to errors in tracing reflectors and identifying their depths. The error in phase sampling of the EM pulse, ϵ_{PW} , is taken to be a function of the wavelength of the pulse, λ . The sampling rate for the data used here varies from 5 ns to 20 ns. We assume a 10 ns resolution when tracking the phase of layer detections and assume this error is normal.

Finally, in the upper part of the ice sheet, a firn layer of less density than glacial ice acts to slow the velocity of the radar signal. To deal with this, we use a firn correction to accurately estimate the depth to radar reflectors. All englacial reflectors of interest in this study are deeper than the firn layer, so a single firn correction—the difference between the ice thickness with and without the firn layer present—is added to layer depths to

correction for the underestimation of depth if the firn layer is not considered. The firn correction, d_{firn} , is treated as a model parameter for which we invert. Based on density measurements at the Byrd ice core site [Gow, 1970], bounds can be placed on the firn layer thickness and therefore the firn correction. We assume the firn correction to be less than the firn layer depth and sample values from a uniform distribution: $p(d_{firn}) \sim U(1 \text{ m}, 65 \text{ m})$.

We assume constant velocities, \vec{v} , in air ($300 \text{ m}/\mu\text{s}$) and ice. The TWTT from the observing aircraft to the surface of the ice sheet is known from interpretation of the surface reflector and the remainder of the signal is assumed to be in glacial ice. The computed depth of each reflector is relative to the ice surface as also measured by the HiCARS radar. While each layer may have depth errors independent of the others, errors in the distance between the surface and the acquisition aircraft are systematic across all observed reflectors in the ice column. Therefore, a randomly sampled error due to the vertical resolution is computed for the ice sheet surface and the same error is applied to all radar reflectors in the column.

2.3. Metropolis Algorithm

At each iteration, the Metropolis sampling algorithm [Metropolis *et al.*, 1953] proposes values for parameters of interest (those with priors in Equation 1). The algorithm accepts or rejects proposed sets of parameter values by comparison between the proposed and previously-accepted likelihood (or “cost”) values. A low cost value represents good agreement between model and observations, reflecting a small model-data misfit. According to the Metropolis algorithm, if the cost associated with proposed parameters is significantly lower than that of the last accepted iteration, the proposed parameter values have a high

probability of being accepted as a more likely solution. Each likelihood function is considered separately and both must represent an adequate solution on a given iteration for the proposed parameters to be accepted.

This process is repeated 100,000 times to create an ensemble of accepted parameter sets. These are used in the forward ice flow model to create an ensemble of age-depth profiles constrained by the combined uncertainty in the volcanic age-depth profile, ice model parameterizations, and TWTT observations. The resulting posterior distribution samples the age uncertainty in the Byrd ice core, providing the first robust uncertainty analysis of the ice core chronology.

There are two likelihood functions under consideration, describing the model-data misfit between reflector depth and age, respectively:

$$p(A_{IC}|D_{IC}, \vec{f}, S) = \exp\left[\frac{-S \sum_{j=60} [A_{IC,j} - A_{m,j}(\vec{f}, D_{IC})]^2}{2\sigma_A^2}\right] + r^6 \quad (5)$$

$$p(TWTT_r|D_r, d_{firn}, v_{ice}) = \exp\left[\frac{-\sum_{i=4} [TWTT_{r,i} - TWTT_{m,i}(D_r)]^2}{2\sigma_{TWTT}^2}\right] \quad (6)$$

In the depth likelihood function, $TWTT_m(D_r)$ is based on the relationship between depth and TWTT as in Equation 4 and $TWTT_r$ is observed by ice-penetrating radar for each reflector, i . To estimate uncertainty in TWTT, we iteratively calculate cost values between estimates of σ_{TWTT} , and a perfect model of TWTT based on Equation 4. Depth errors are assumed multivariate normal and the variance is proportional to the number of degrees of freedom as discussed in Appendix ??.

In the age likelihood function, $j = 61$ represents the 61 volcanic events in the record used in this study (see Appendix ??). A_m comes from solutions to the forward ice flow model.

A regularization term, r , is used to penalize large variability in the sampled accumulation rate function input to the ice flow model. Due to poor knowledge of uncertainty in the volcanic record, we assume a baseline age uncertainty, σ_A , of 1%. A hierarchical Bayes approach then incorporates a precision parameter, S , which inverts for age uncertainty in our model as described in *Jackson and Huerta [2016]*:

$$S = Ga\left(\frac{k_e}{2} + \alpha, E_m + \beta\right) \quad (7)$$

Parameters α and β are assumed to be 1 as in the case for a noninformative gamma prior. The number of degrees of freedom, k_e , is assumed to be less than j due to covariation in the age and depth of ice. Because we do not know the value of k_e a priori, we assume $k_e = \frac{j}{2}$ as discussed in Appendix C. E_m is simply the model-data misfit term from Equation 5:

$$E_m = \frac{\sum_j [A_{IC,j} - A_{m,j}(\vec{f}, D_{IC})]^2}{2\sigma_A^2} \quad (8)$$

The precision parameter is used to account for uncertainty in addition to the assumed 1% when finding an optimal age solution. New values of S are proposed for each Metropolis iteration, effectively estimating reflector age uncertainty given the choice of parameter solution for each iteration.

3. Updated Byrd ice core chronology

The age-depth distribution derived for the Byrd ice core site using these methods is shown in Figure 4. This updated chronology has been trained on previously-derived ECM estimates of volcanic events observed in the Byrd ice core, but also includes estimates of uncertainty in this data, radar observations, local ice flow parameters, and local accumulation rate.

Corresponding probability density functions generated by the metropolis algorithm sample uncertainty in the age and depth for each of four radar reflectors observed near the Byrd ice core. The age of the observed reflectors increases dramatically with depth. These observed reflectors span to before the Last Glacial Maximum, with the oldest and deepest observed reflector dated to 26.1 ± 1.59 ka.

We assume radar reflectors to be isochronous such that their age should be the same whether observed at the Byrd ice core or the WAIS Divide ice core. To compare between the two ice cores, we use Halliburton's Landmark seismic interpretation software to track radar reflectors through central WAIS via existing radar survey flight lines shown in Figure 2.2. We confirm the ages we compute for all four reflectors at the Byrd ice core site agree to within 2σ uncertainty with the independently-derived WAIS Divide ice core chronology (Figures 3b,c and 4).

Estimated values of the model parameters can be seen in Appendix C. As expected, estimates of the depth of the four radar reflectors at each iteration (Figure ??) are correlated to each other because knowledge of the depth and age of each layer informs the relative depth and age of all other reflectors. To ensure the accumulation rate as a function of depth is not unrealistically variable, our method includes a regularization term. The resulting accumulate rate profile is shown in Figure C.3. The accumulation rate profiles more closely resemble a climatic record, for which the accumulation rate was lower during the Last Glacial Maximum.

4. Discussion

For this study, we employ a simplified ice flow model which does not include upstream corrections and assumes one-dimensional vertical strain and constant horizontal strain

rate in the upper part of the ice sheet. Below, the model includes shear layer in which horizontal strain decreases linearly to the bed which is allowed to slide. We do not include a separate term for basal melting, which is likely occurring at this site because liquid water was observed at the bed during drilling. Despite this simplification, our results agree with two independent ice core chronologies.

The four reflectors in this study were chosen as a representative sample of the ice column and for their brightness and continuity. It is possible to use this method to date additional englacial reflectors observed using radar in this area. However, the usefulness of such dates only extend as far as the isochronous reflectors can be traced. This method is less helpful for dating discontinuous reflectors, though it could inform relative ages for reflectors seen coincident with dated reflectors but which can be traced only over short distances.

All such dating efforts should agree to within uncertainty at multiple ice core locations as in *Cavitte et al.* [2016]. We see agreement within 2σ between our estimated reflector ages at the Byrd ice core and those observed at the WAIS Divide ice core, though the mean of the latter estimates tend younger than those at the Byrd ice core site. It is unclear why this is the case, though it may be attributable to additional missing uncertainties in drilling of the Byrd ice core. As an early deep-drilling effort, less sophisticated technology may have led to more deviations in the drilling direction than reported, for example. Deviations from vertical may lead to a longer core sample than the true ice thickness and may skew the reported volcanic chronology (as measured from the ice core) to be older than it really is.

Our method is sensitive to the possibility that uncertainty in the estimate of different parameters might be correlated. This is consistent with expectations that parameter

values will covary with depth. Because there is not independence between parameters, we must make an assumption about the effective number of degrees of freedom in the problem. For our age likelihood and estimation of S , we assume $k_e = 50\%$ of the number of volcanic data points and do not expect this to change the mean estimates of reflector age and depth, as shown in Appendix C. However, the choice of k_e does have an influence on the uncertainty as indicated in Equation 7.

- what would it take to calculate?
- why didn't last method work?

5. Conclusion

We derive an updated chronology for the Byrd ice core which includes estimates of uncertainty in ice flow parameters and ice properties in the region of Marie Byrd Land, West Antarctica, for which additional observations from radar surveys are just becoming available. Such radar observations reveal englacial stratigraphy indicative of past ice flow, but require dating to put constraints on interpretations of ice dynamics. The Byrd ice core is strategically located to connect the WAIS divide to the ice streams of the Siple Coast and the Marie Byrd Land icecap, but its chronology has lacked robust estimates of uncertainty until now.

In addition to estimating uncertainty in the chronology for the full ice column, we estimate the age and depth of four radar reflectors observed in central West Antarctica. Our estimates of the reflector age-depth are confirmed by comparison to the same reflectors dated using the WAIS Divide ice core chronology [Buizert *et al.*, 2015].

In the process of updating the Byrd ice core chronology, we also compute self-consistent estimates (with uncertainty) of local ice characteristics, such as the accumulation rate as

a function of depth, the firn correction, and the velocity of EM waves in ice. Our method also samples uncertainty in estimates of depth from radar observations. These parameter estimates can be used to inform ice sheet modeling efforts in this area and for other studies of paleo ice flow through the Last Glacial Maximum.

Our results indicate the oldest continuous radar reflector dateable using existing ice cores and radar surveys in West Antarctica is located at $\sim 70\%$ ice depth at the Byrd ice core site and dates to $\sim 26\text{ka}$. The same reflector is observed at $\sim 80\%$ ice depth in the WAIS Divide ice core. While the Byrd ice core has been isotopically dated to as old as $\sim 94\text{ka}$ [Blunier and Brook, 2001], continuous radar reflectors do not extend deep enough in this region to leverage the ice core to date older aspects of the ice geometry in the central WAIS.

Appendix A: Metropolis Evaluation

The metropolis algorithm was evaluated for 450,000 iterations, with the first 10,000 discarded as “burnin” iterations, during which the model was experiencing transient behavior. Such a large number of iterations allows for convergence of all parameters to their best solutions. Our method is based on a markov chain, such that the proposed parameter values for each iteration depend on the values from the last accepted iteration according to:

$$\begin{aligned} \textit{delta} &= \textit{Range}(\textit{Prior}) \\ \textit{Proposal}_i &= \textit{Accepted}_{i-1} + \textit{dp} \cdot (0.5 - \textit{rand}) \cdot \textit{delta}; \end{aligned} \tag{A1}$$

where \textit{delta} is the range allowed by the uniform prior for each parameter and \textit{rand} is a random number between 0 and 1. $\textit{Proposal}_i$ is the value of a parameter for iteration i and $\textit{Accepted}_{i-1}$ is the previous value of that parameter accepted by the algorithm. To

more efficiently explore parameter space, proposed parameters were selected with step sizes $dp_{Age} = 0.1$ and $dptWTT = 0.1$ for those parameters associated with each likelihood in Equation 1.

The evaluation of the two likelihood functions (i.e. “cost”) are independently accepted according to each function’s metropolis probability during each iteration. The accepted solutions for each cost, depth, and age are shown in Figure A.5. As seen in the figure, these cost values show little trend aside from occasional positive departures from the mean as the model explores parameter space.

Appendix B: Regularization

Sampling accumulation rate parameters along the depth profile is inefficient and problematic because many proposed solutions are unrealistically variable. We expect the mean accumulation rate over time (and therefore depth) changes slowly and continuously. To improve our accumulation rate solutions, we regularize the likelihood of reflector age. A regularization parameter is added to the age cost term which punishes proposed accumulation rate profiles which are highly variable relative to a solution computed with no regularization and smoothed over a moving 600-m depth window. This window size is chosen because it is the smallest interval over which the data can be smoothed given the 200-m bin size of the accumulation rate parameters.

The regularization term, r is the ratio of the variance of a proposed set of accumulation rates to the variance of the smoothed, non-regularized accumulation rate profile. Values of the regularization term for accepted parameter solutions are shown in Figure B.1. The regularization is weighted as r^6 when included in the calculation of the age cost (Equation 5) to sufficiently reduce variability in the accumulation rate profile.

Appendix C: Degrees of freedom and parameter correlation

As we invert for model parameter values, we anticipate the data points used to constrain our likelihood functions – sourced from radar observations and a Byrd ice core volcanic chronology – are not independent of one another. As a result, we expect the number of degrees of freedom to be less than the number of data points available. While we do not know the number of effective degrees of freedom, k_e , we explore the sensitivity of our results to our choice of k_e (Figure C.1). We find that our choice does not significantly impact the mean estimates of age or depth for our radar reflectors. In lieu of more information about the degrees of freedom, we choose to assume $k_e = \frac{N_{data}}{2} = 30.5$ because convergence on the accumulation rates are strong and the rate at which the algorithm finds solutions is reasonable.

Figure C.2 shows the results of inverting for several model parameters in this problem, including flow parameters such as q as well as ice property parameters such as v_{ice} . The results show the parameters are not correlated with one another and do seem to converge to most-likely solutions.

Accumulation rate is divided into 10 parameters, each covering a depth bin of ~ 200 m. This allows for variation in the accumulation rate over time, as expected. The resulting accumulation rate profiles are shown in Figure C.3. As discussed previously and further in Appendix B, these profiles have been regularized to preferentially select those which do not exhibit unrealistic variability. In Figure C.3, they have been additionally sorted by cost to demonstrate the relative quality of the accepted solutions.

To further explore the accumulation rate solutions, we look at the accepted parameter values and their convergence over all iterations. As seen in the right side of Figure C.4, the

accumulation rate solutions do not converge as readily as other parameters, leaving wider distributions exhibiting more uncertainty in our estimates of accumulation rate. This may mean that our priors play an important role in estimating the value of accumulation rate and therefore the result could be improved with a more informative prior. This is particularly true at the bottom of the ice column, where neither volcanic chronology data nor radar data is available to constrain the accumulation rate.

We see correlation between some accumulation rate parameters (left side of Figure C.4). This may indicate we could have combined these accumulation rate depth bins. Figure C.5 shows a correlation matrix between pairs of accumulation rate parameters. Along the diagonal are histograms of each accumulation rate parameter. Pairs of accumulation rate parameters tend to not be very correlated and only one pair of accumulation rate parameters has $R^2 > 0.5$. In general, R^2 values are highest between accumulation rates in the lower part of the ice column, where parameter values are more difficult to constrain due to a lack of data and flatter age-depth profile.

Acknowledgments. Robert, Shubhang, Arami, Bekah, Varun, Benj, Chad, Marie, etc.

References

- Blunier, T., and E. J. Brook, Timing of millennial-scale climate change in antarctica and greenland during the last glacial period, *Science*, 291(5501), 109–112, doi: 10.1126/science.291.5501.109, 2001.
- Buizert, C., et al., The wais divide deep ice core wd2014 chronology—part 1: Methane synchronization (68–31 ka bp) and the gas age–ice age difference, *Climate of the Past*, 11(2), 153–173, 2015.

- Cavitte, M. G., D. D. Blankenship, D. A. Young, D. M. Schroeder, F. Parrenin, E. Lemeur, J. A. Macgregor, and M. J. Siegert, Deep radiostratigraphy of the east antarctic plateau: connecting the dome c and vostok ice core sites, *Journal of Glaciology*, 62(232), 323–334, 2016.
- Cuffey, K. M., and W. S. B. Paterson, *The physics of glaciers*, Academic Press, 2010.
- Fretwell, P., et al., Bedmap2: improved ice bed, surface and thickness datasets for antarctica, *The Cryosphere*, 7(1), 2013.
- Fujita, S., T. Matsuoka, T. Ishida, K. Matsuoka, and S. Mae, A summary of the complex dielectric permittivity of ice in the megahertz range and its applications for radar sounding of polar ice sheets, *Physics of Ice Core Records*, pp. 185–212, 2000.
- Gow, A. J., Preliminary results of studies of ice cores from the 2164 m deep drill hole, byrd station, antarctica, *IAHS Publ*, 86, 78–90, 1970.
- Gow, A. J., H. T. Ueda, and D. E. Garfield, Antarctic Ice Sheet: Preliminary Results of First Core Hole to Bedrock, *Science*, 161, 1011–1013, doi:10.1126/science.161.3845.1011, 1968.
- Hammer, C., H. Clausen, and C. Langway, 50,000 years of recorded global volcanism, *Climatic Change*, 35(1), 1–15, 1997.
- Holt, J. W., D. D. Blankenship, D. L. Morse, D. A. Young, M. E. Peters, S. D. Kempf, T. G. Richter, D. G. Vaughan, and H. F. J. Corr, New boundary conditions for the West Antarctic Ice Sheet: Subglacial topography of the Thwaites and Smith glacier catchments, *Geophysical Research Letters*, 33, L09502, doi:10.1029/2005GL025561, 2006.
- Jackson, C. S., and G. Huerta, Empirical bayes approach to climate model calibration, *Geoscientific Model Development Discussions*, 2016, 1–19, doi:10.5194/gmd-2016-20,

2016.

Luyendyk, B. P., D. S. Wilson, and C. S. Siddoway, Eastern margin of the Ross Sea Rift in western Marie Byrd Land, Antarctica: Crustal structure and tectonic development,

Geochemistry Geophysics Geosystems, 4, doi:10.1029/2002GC000462., 2003.

Metropolis, N., A. W. Rosenbluth, M. N. Rosenbluth, A. H. Teller, and E. Teller, Equation of state calculations by fast computing machines, *The Journal of Chemical Physics*, 21(6), 1087–1092, doi:<http://dx.doi.org/10.1063/1.1699114>, 1953.

Millar, D., Acidity levels in ice sheets from radio echo-sounding, *Ann. Glaciol.*, 3, 199–203, 1982.

Morse, D. L., D. D. Blankenship, E. D. Waddington, and T. A. Neumann, A site for deep ice coring in west antarctica: results from aerogeophysical surveys and thermo-kinematic modeling, *Annals of Glaciology*, 35(1), 36–44, 2002.

Peters, M. E., D. D. Blankenship, and D. L. Morse, Analysis techniques for coherent airborne radar sounding: Application to West Antarctic ice streams, *Journal of Geophysical Research (Solid Earth)*, 110, B06303, doi:10.1029/2004JB003222, 2005.

Schwander, J., J. Jouzel, C. U. Hammer, J.-R. Petit, R. Udisti, and E. Wolff, A tentative chronology for the EPICA Dome Concordia ice core, *Geophysical Research Letters*, 28, 4243–4246, doi:10.1029/2000GL011981, 2001.

Young, D. A., D. D. Blankenship, and J. W. Holt, GIMBLE: Geophysical Investigations of Marie Byrd Land Evolution: a new airborne survey of the linchpin of the West Antarctic, *WAIS Workshop 2012*, 2012.

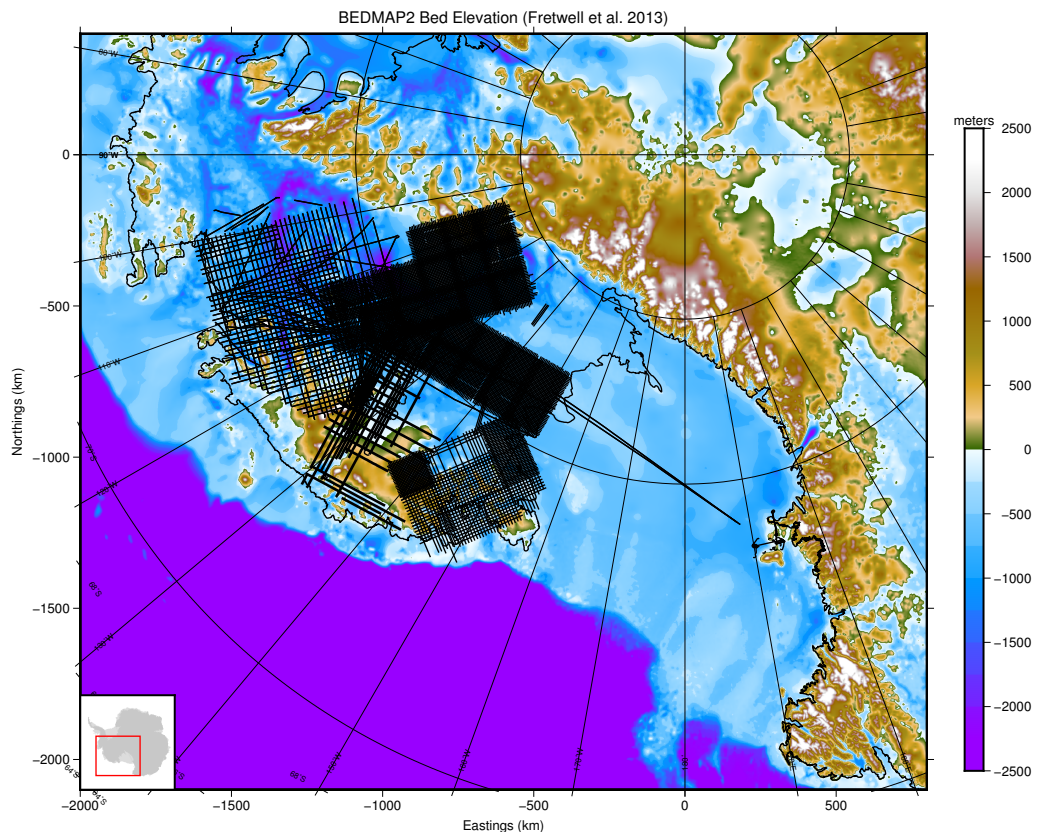


Figure 1. Map of central West Antarctic with available airborne geophysical radar surveys (black lines) and (will be updated to have: WAIS Divide and Byrd ice core locations (blue triangles) overlain. Gray shading is surface elevation [Fretwell *et al.*, 2013].

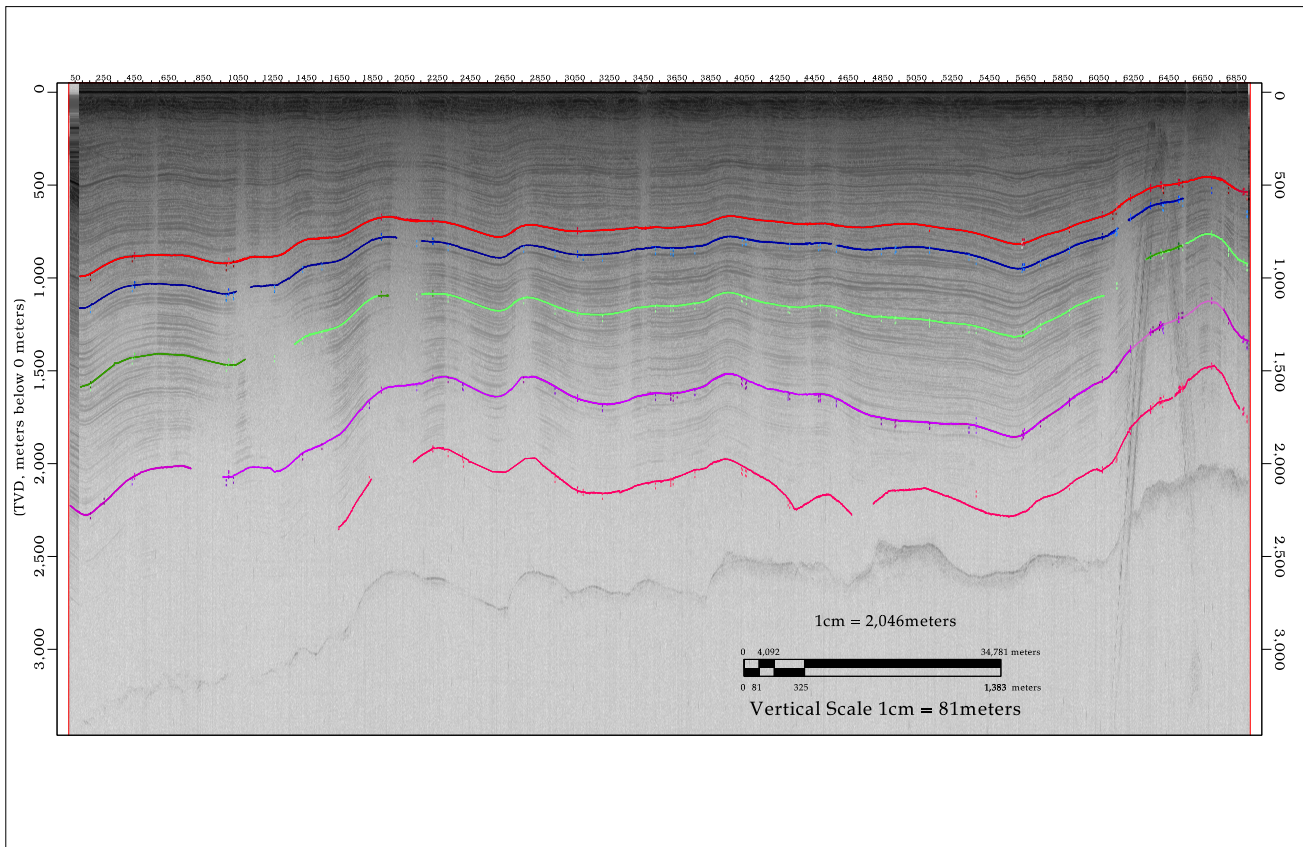


Figure 2. Radargram showing reflectors of interest near the Byrd ice core.

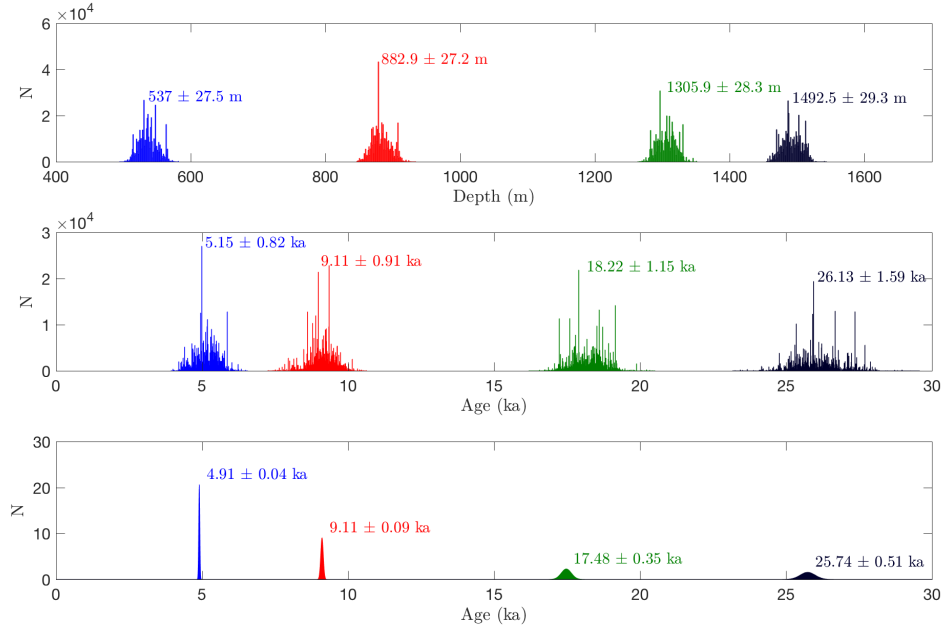


Figure 3. Depth (top) and age (middle) distributions of 4 radar reflectors at the Byrd ice core and the age distribution of the same 4 reflectors at the WAIS Divide ice core (bottom). The width of the age and depth histograms for the Byrd ice core chronology represent uncertainty estimated by the methods used here. The WAIS Divide ice core distributions are recreated from the WAIS Divide ice core chronology *Buizert et al.* [2015] and are used as an independent check on our estimation of the age-depth distribution at the Byrd ice core.

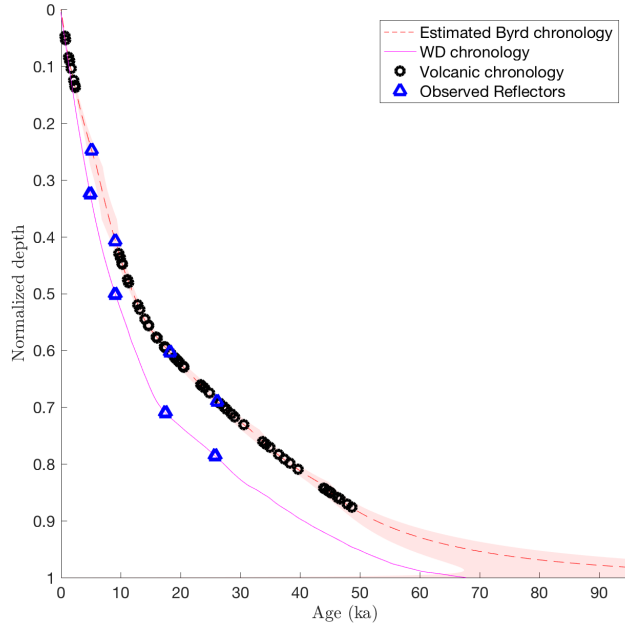


Figure 4. Modeled age-depth relationship with uncertainty compared to measured volcanic chronology from *Hammer et al.* [open circles; 1997]. The WAIS Divide ice core chronology [*Buizert et al.*, 2015] is shown in green. Blue triangles show the age-depth of 4 radar reflectors at each of the Byrd and WAIS Divide ice cores; these reflectors are assumed isochronous and so expected to be the same age at either ice core.

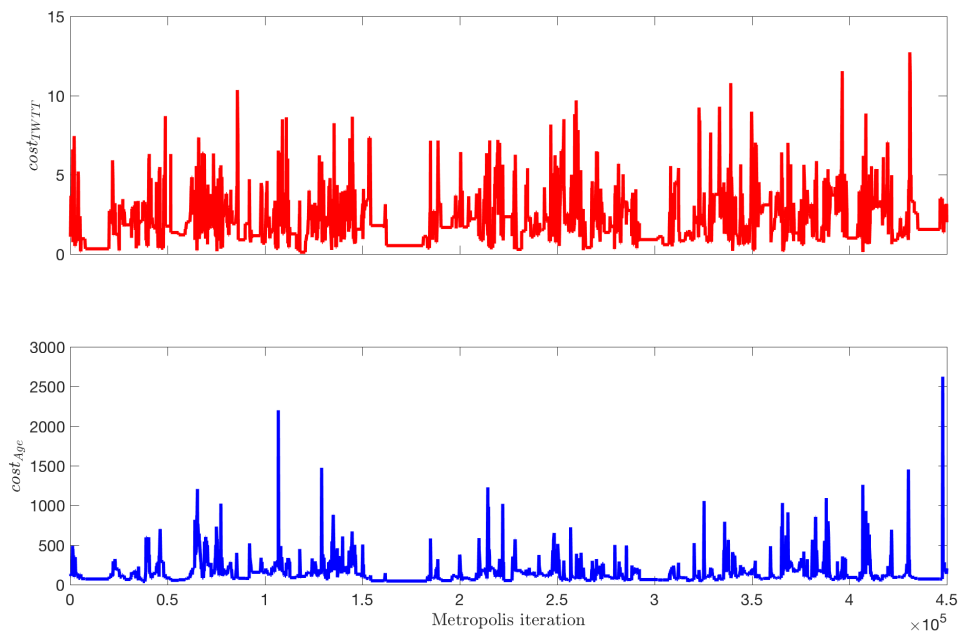


Figure A.5. Cost of the age and depth likelihood functions at each accepted iteration.

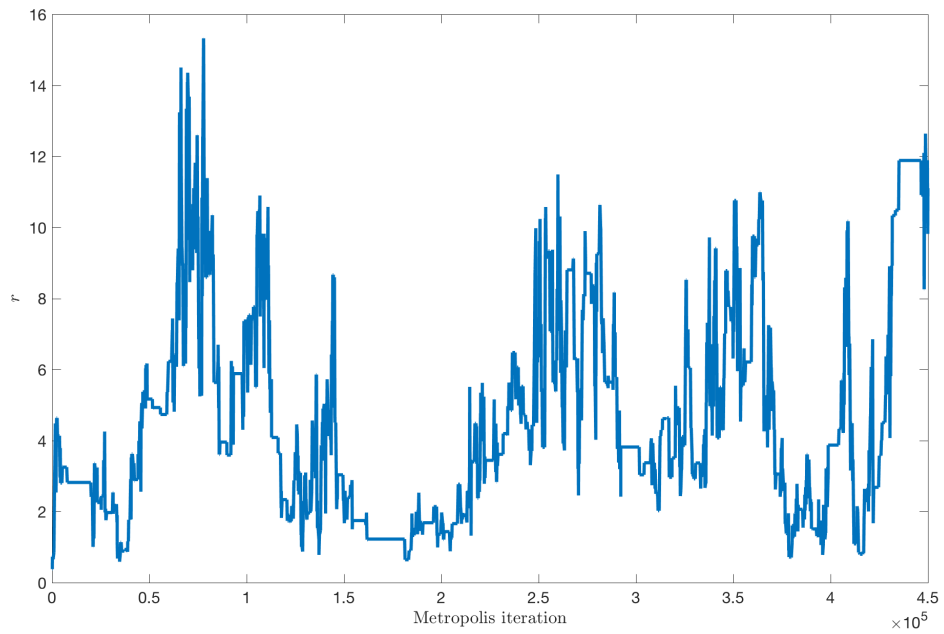


Figure B.1. Values of the regularization parameter at each accepted metropolis iteration.

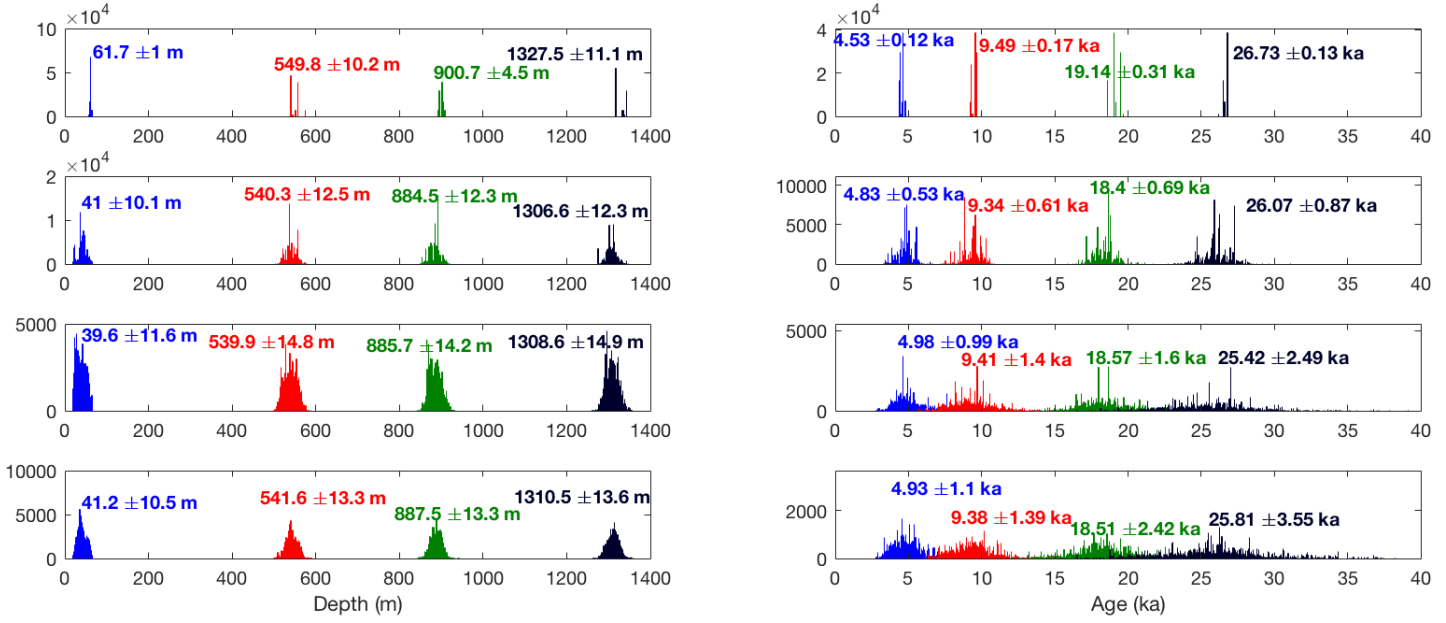


Figure C.1. Comparison of results for reflector age and depth assuming a range of k_e values. All agree to within uncertainty.

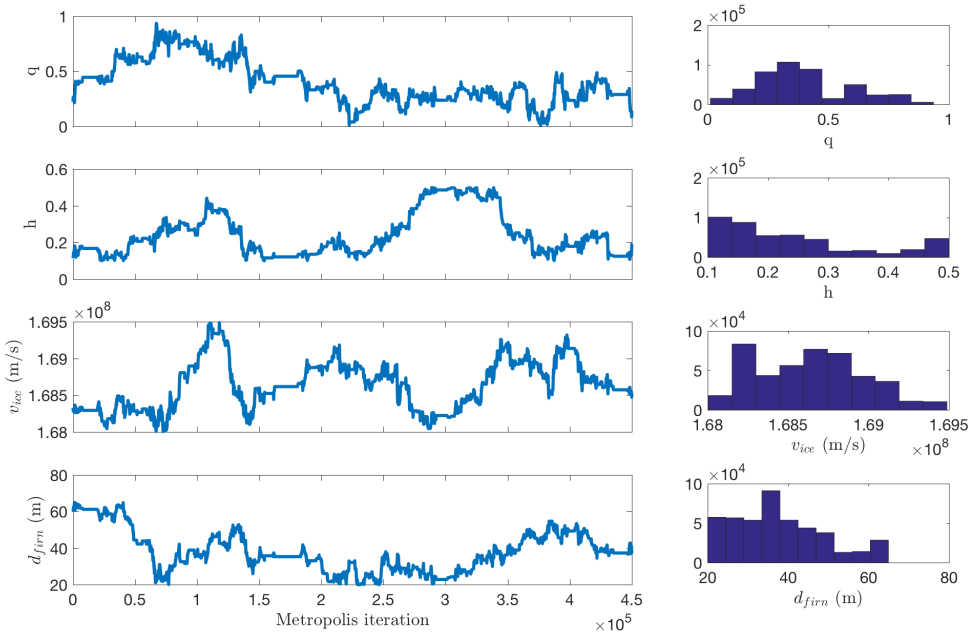


Figure C.2. Left: Flow parameter values at each accepted Metropolis iteration for parameters q (top), h , v_{ice} , and d_{firn} (bottom). The parameter values do not appear correlated Right: Histograms of the parameter values shown in the left column. Histograms show the parameter values converging.

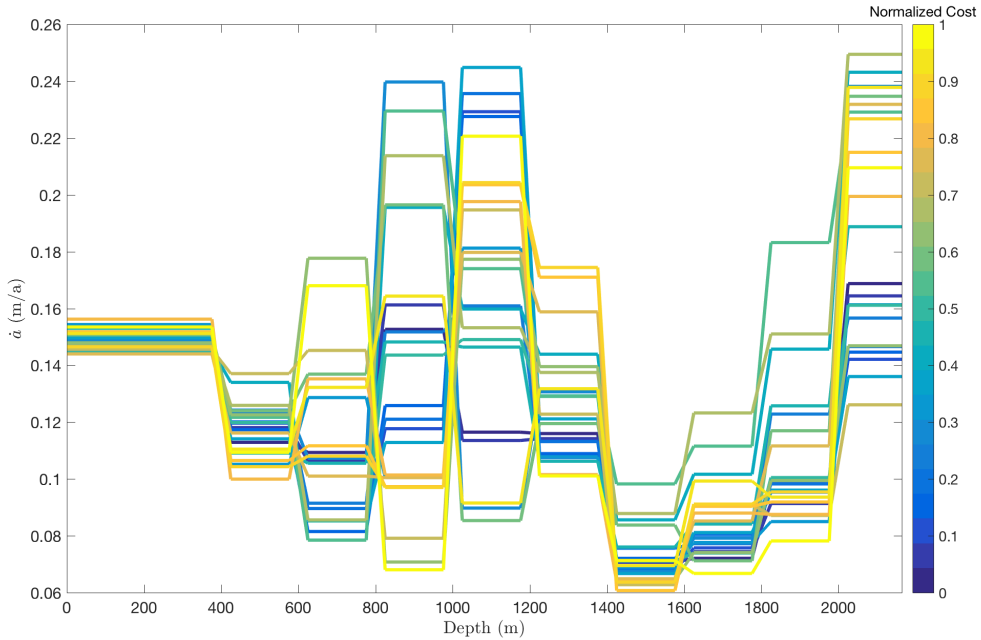


Figure C.3. Accumulation rate as a function of ice depth colored by cost value for the estimated parameter values. (Accumulation rate series associated with lower cost are expected to be solutions.) Accumulation rate is estimated in 10 depth bins at ~ 200 m depth intervals. Transitions between these intervals have been smoothed in this figure for each of viewing.

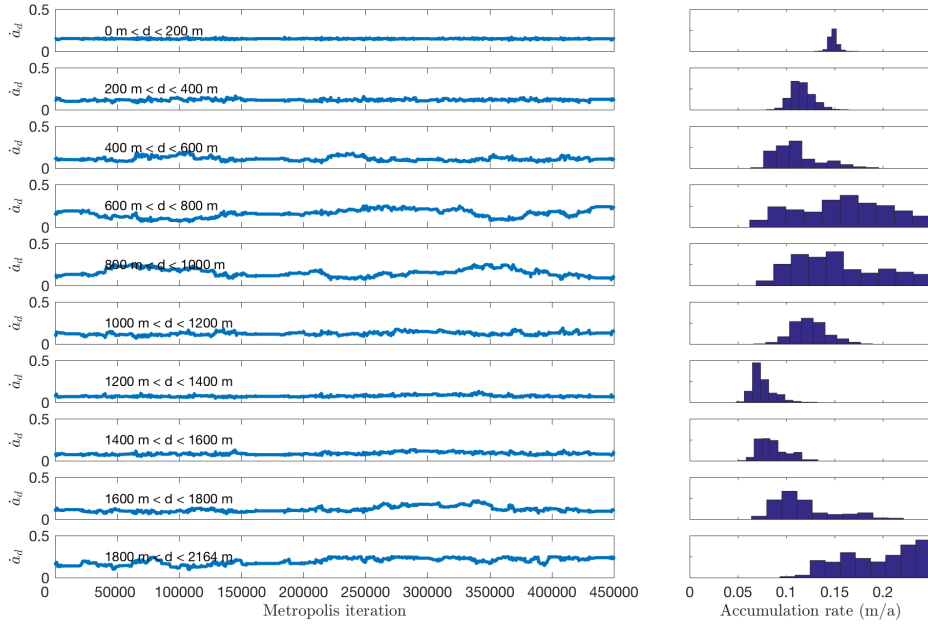


Figure C.4. Left: Values of each accumulate rate parameter (in each of 10 depth bins, shallowest at top). Right: Histograms of the parameter values at left. Certain depth bins appear to be correlated and the histograms of values are wider, indicating the accumulation rate parameters are slower to converge and more uncertain.

Table 1. Depth and age mean, median, and uncertainty for four radar reflectors near Byrd Station, West Antarctica used in this study. The radar-observed two-way travel time (TWTT) for each reflector is also shown.

Reflector	TWTT (μ s)	Depth (m)		Age (a)	
		Mean	2σ	Mean	2σ
1	8.44	537	27.5	5150	820
2	12.54	882.9	27.2	9110	910
3	17.55	1305.9	28.3	18220	1150
4	22.42	1492.5	29.3	26130	1590

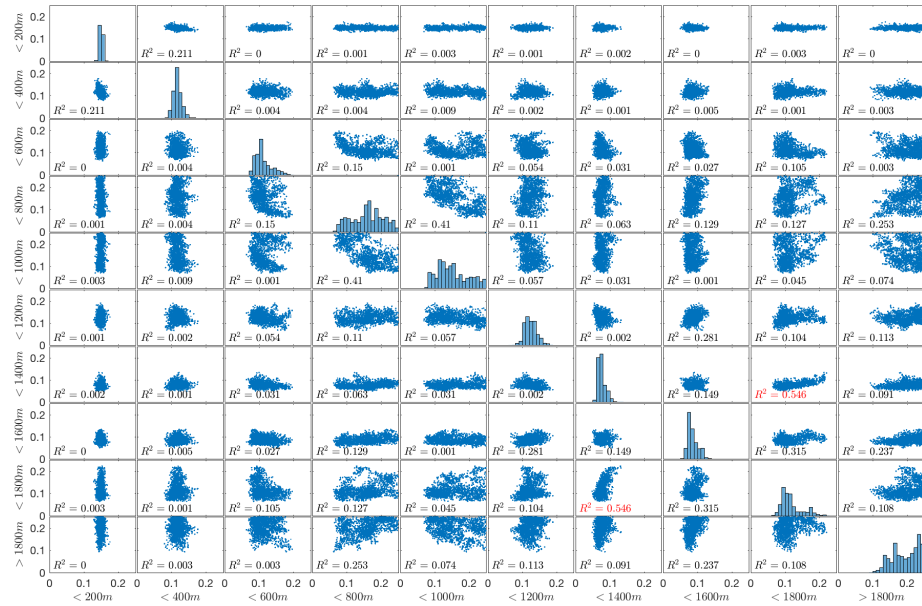


Figure C.5. Correlation of each accumulation rate parameter with every other accumulation rate parameter. Histograms of each accumulation rate are shown along the diagonal. Pairs of parameters with $R^2 > 0.5$ have their correlation coefficients shown in red.